Applied Scientific Research **46**: 291–307, 1989.

The measurement of $\langle U \rangle$, $\langle V \rangle$ and $\langle uv \rangle$ inside the turbulent spot using conditionally sampled hot-wire anemometer signals

F.C. BOSVELD,[1] J.J.M. VAN HAREN[2] & F.G.J. ABSIL[3]

Laboratory for Aero- and Hydrodynamics, Delft University of Technology, The Netherlands; present addresses: [1]Royal Netherlands Meteorological Institute, P.O. Box 201, 3730 AE de Bilt, The Netherlands; [2]Netherlands Institute for Sea Research, P.O. Box 59, 1790 AB den Burg, The Netherlands; [3]p/a Saclant ASW Research Centre, Viale San Bartolomeo 400, 19026 La Spezia, Italy

Received 26 November 1987; accepted in revised form 1 April 1989

Abstract. By means of a tripping wire turbulent spots are generated in a conditionally stable laminar boundary layer along a flat plate in a low-turbulence windtunnel. At several vertical and lateral positions the streamwise (U) and vertical (V) velocity components of the spot are measured using an X-shaped hot wire anemometer. The spot's leading edge (LE) and trailing edge (TE) are determined by a high frequency detection criterion.

The derived ensemble averaged shear stress $\langle uv \rangle$ shows a remarkable plateau over the last 3/4 of the spot length and over about 1/2 of the spot width, approximately independent of the height above the plate. The measurements suggest that the velocities of the LE and the TE can be explained by simple advection of the active turbulent region. Other mechanisms seem to be responsible for the lateral spread of the spot, as is suggested by the measurements outside the plane of symmetry.

1. Introduction

Over the past ten years the interest in artificially created turbulent spots has increased to find the mechanisms acting in a turbulent boundary layer. Especially the hypothesized resemblance between coherent structures in a fully turbulent boundary layer and spots has inspired several investigations on the structure of the turbulent spot.

In general, two experimental approaches have been applied, first, qualitatively by smoke- or dye-visualization of individual spots and second, quantitatively through registration of conditionally sampled and ensemble averaged velocity signals obtained by either hot-wire or laser-Doppler anemometry. The first approach shows the individual spot as a region of high turbulence intensity. However, such a picture does not contain any statistically relevant information. The second approach overcomes this difficulty, but intense high-frequency disturbances are suppressed due to the

ensemble-averaging. For more insight in the structure of the turbulent spot, the two methods should be combined and accompanied by numerical simulations [6].

Wygnanski et al. [12] investigate the averaged velocity $U_{TE} = 0.5 \cdot U_0$. The velocity field of the spot and its shape. They find that the shape of the spot is independent of its creation mechanism when it is observed sufficiently downstream of its creation point. Its center moves at a velocity of $0.65 \cdot U_0$ (U_0 denotes the free stream velocity). The leading edge velocity $U_{TE} = 0.5 \cdot U_0$. The deviation from the undisturbed U-velocity is positive near the wall ($y < 0.3\,h$; h being the spot height) and negative further away. For $y > 0.1$ h the velocity perpendicular to the wall (V-velocity) is directed downward near the leading edge (LE) and upward near the trailing edge (TE). The laterally directed W-velocity in the spot points out of the plane of symmetry everywhere and attains its maximum at about 2/3 of the half spot-width. Near the plane of symmetry a region of low turbulence activity trails the spot [12]. The spreading angle of the spot is 10 [8, 13].

Itsweire and van Atta [5] calculate an ensemble averaged spot from hot-wire measurements of the U- and W- velocity components. They describe a "statistically most probable spot" which contains four smaller scale coherent eddies. However, the entrainment by these eddies is not sufficient to explain the spot growth. Their measurements of the W-velocity outside the plane of symmetry globally show the same results as described in [12].

The shear stress $\langle uv \rangle$, which is responsible for the large momentum exchange in the spot, is measured in the plane of symmetry by [2]. Their observations show a spot which contains a highly active region near the L.E. and an $\langle uv \rangle$ negative throughout the spot.

According to [3] spotgrowth is conical from a suitably chosen origin. This is contradicted in [1, 2], who scale the spot in the vertical direction with the height of the turbulent boundary layer. Gad-el-Hak et al. [5] conclude from a visualization study that lateral spotgrowth is not affected by the classical entrainment mechanism but is caused by a destabilization of the laminar flow due to the presence of pressure waves.

Wygnanski et al. [11] show that outside the plane of symmetry the spot is trailed by Tollmien-Schlichting waves. They suggest a regeneration process of the spot caused by breakdown of these waves. However, a visualization study by Chambers and Thomas [4] suggests that there is no interaction between the spot and its trailing waves.

Since the shear stress $\langle uv \rangle$ plays an important role in the dynamics of the ensemble-averaged spot, it is felt that knowledge is missing about the signature of the $\langle uv \rangle$-field, especially outside the plane of symmetry. The two velocity components U and V were therefore conditionally sampled in

a windtunnel using hot-wire anemometry and processed on a computer to obtain an ensemble averaged distribution. The measurements resulted in the description of a qualitative model based on the $\langle uv \rangle$-distribution, which can explain the ensemble-averaged $\langle U \rangle$ and $\langle V \rangle$ velocity fields within the spot.

2. Experimental set-up

The measurements are performed in a low-speed, low turbulence intensity, closed-circuit windtunnel at the laboratory for Aero- and Hydrodynamics of Delft University of Technology. The test section (Fig. 1) is 2.70 m long, 0.40 m wide and 0.60 m high. During the experiments the free stream velocity is set at 8.35 ± 0.01 m/s. The temperature in the section is kept constant within 31.5 ± 0.1°C, which is slightly above maximum laboratory temperature. A glass plate (hereafter called "the wall") 1.70 m long is mounted in the test section. A left-handed orthogonal coordinate system is defined with its origin at the center of the upstream edge of the wall. The x-axis points downstream, the y-axis is normal to the wall. The free stream longitudinal turbulence intensity is less than $0.001 \cdot U_0$. The glass plate is adjusted to achieve zero pressure gradient over the experimental section $(2/\varrho U_0^2) \cdot (\partial p/\partial x) < 4 \times 10^{-3}\,\mathrm{m}^{-1}$. Velocity profiles for the undisturbed boundary layer above the wall are measured at $x = 0.85$ m. They agree with the Blasius profile within 0.6% of the free stream velocity down to $\sqrt{(vx/U_0)} \approx 1$ ($y \approx 1.3$ mm), where v is the kinematic viscosity. Below this level wall-interference of the hot-wire becomes important. Turbulent

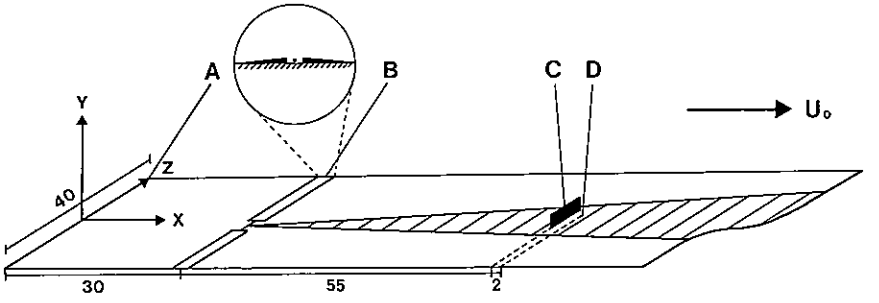

A leading edge of the wall
B tripping wire in dike
C measuring stations
D position reference wire

Fig. 1. Test section (dimensions in cm).

spots are generated in the boundary layer above the wall by means of a 0.12 mm thick tripping copper wire, which is mounted parallel to the z-axis at $x = 29.5$ cm. The wire is embedded in a 0.6 mm high dike except for a 2 cm wide gap around $z = 0$ m. The dike itself does not disturb the laminar flow. At intervals of 4 seconds the wire is set in motion for a period of 25 ms, during which it vibrates in vertical direction over approximately two periods with an amplitude of less than 0.3 mm. The point-like flow disturbance, thus generated, grows downstream to become a turbulent spot. Reproducibility of the spot can be quantified by the variation of the spotlength relative to the ensemble mean, which amounts up to 10% (5 ms).

On the wall a singe hot-wire probe is positioned at $x = 0.89$ m, $y = 7$ mm, $z = 5$ mm, close to the X-wire probe. This "reference-wire" is used for aligning in time the spot ensembles measured at different $y - z$ positions.

To measure two velocity components close to the wall a special X-wire probe is constructed following the design criteria of Strohl and Comte-Bellot [9]. The two tungsten wires, 5 μm thick and 1 mm long, are mounted in such a way that measurements can be performed at 0.7 mm from the wall.

Due to the configuration of the X-wire probe the $y = 0$ mm point is difficult to find directly. As the measured laminar velocity profiles are in excellent agreement with the Blasius profile, the y-position of the probe at each x-position can be determined by fitting the profiles measured to theoretical ones. The y-position determined in this way and the one determined with mechanical (micrometer) equipment agreed better than 0.02 mm for a single wire probe. For an X-wire configuration we estimate the accuracy to be better than 0.1 mm. Calibration of the X-wire anemometer is performed in two steps: a velocity calibration is followed by a yaw calibration. Both calibrations are executed in a uniform and laminar flow field. During the velocity calibration both wires are in their working position, i.e. the wires are positioned at angles of $\pm 45°$ to the mean flow direction. A third order polynome is used to relate velocities with anemometer voltages. To correct for axial wire cooling effects yaw calibration is performed at three free stream velocities ($U_0 = 5.0$, 6.5 and 8.5 m/s) at five different probe angles to the free stream velocity direction ($\varphi = \pm 25°$, $\pm 12.5°$, $0°$). Differences between velocities measured with the X-wire and the true velocities derived from Pitot-tube measurements amounts to 4% (at $\varphi = 0°$) and 11% (at $\varphi = \pm 25°$) before yaw calibration and to 1% (at $\varphi = 0°$) and 4% (at $\varphi = \pm 25°$) after yaw calibration. However, the latter errors are still of the same order of magnitude as the values of V ($V/U_0 < 0.05$) and consequently will have their effect on the accuracy of the V-measurements. On the other hand, it must be kept in mind that these errors are not random, but that they are a function of flow direction and small for $\varphi \approx 0°$.

This implies that the zero-points as well as the characteristics of the V-component will be preserved.

Our yaw-calibration method is less accurate than the so-called "lookup table" method [14], but has the advantage of being less computer-time consumptive. Probably another source of errors is calibrating in uniform and laminar flow, while the measurements are taken in a highly sheared and turbulent environment where flow distortions due to the probe are unknown. This source of errors has not been investigated.

3. Data reduction

The hot-wire signals are sampled by a 12 bits A–D convertor and processed on a DEC PDP-11/34 minicomputer. Sampling starts about 20 ms after spot generation. The two X-wire signals and the reference-wire signal are sampled consecutively at a rate of 15 kHz for 230 ms and saved on magnetic disk.

For each x, y and z position of the X-wire 60 spots are recorded, hereafter called an ensemble. Further processing, i.e. LE and TE detection, alignment of the spot signals and ensemble averaging, is performed digitally. In determining LE and TE a method analogous to that of [12] is applied. The spot signal is high-pass filtered at a cutt-off frequency of 500 Hz, resulting in a zero signal outside the spot, see Fig. 2. Next, the signal is squared and smoothed with an exponential low-pass filter (-3 dB at 200 Hz). The resulting signal is suitable for a first estimate of the LE and TE by applying a level-criterion. From the length and the maximum height of the processed signal, a characteristic gradient is derived. This gradient is used for a further refinement of the LE and TE detection by searching the position where the gradient of the signal equals this gradient. Spot signals are rejected if the spot length is out of a pre-defined range ($\approx 1\%$ of the spots).

To suppress spreading over and avoid unwanted introduction of apparent turbulence in an ensemble, due to variation in lengths of the individual spots, the following ensemble averaging procedure was used. After the detection of the LE's and TE's in an ensemble, two ensemble averages are calculated: an LE-average by aligning the LE's and a TE-average by aligning the TE's. The two averages were combined with weight-functions which favour the LE-average at the LE and the TE-average at the TE. The length of the ensemble averaged spot equals the mean spot length.

An important question is how many realisations N are needed to arrive at a good ensemble average. In Fig. 3, ensemble averages of the U-velocity are shown for $N = 90$ and for $N = 20$. It is clear that the global shape of the spot is already apparent at $N = 20$. The amplitude of the small scale

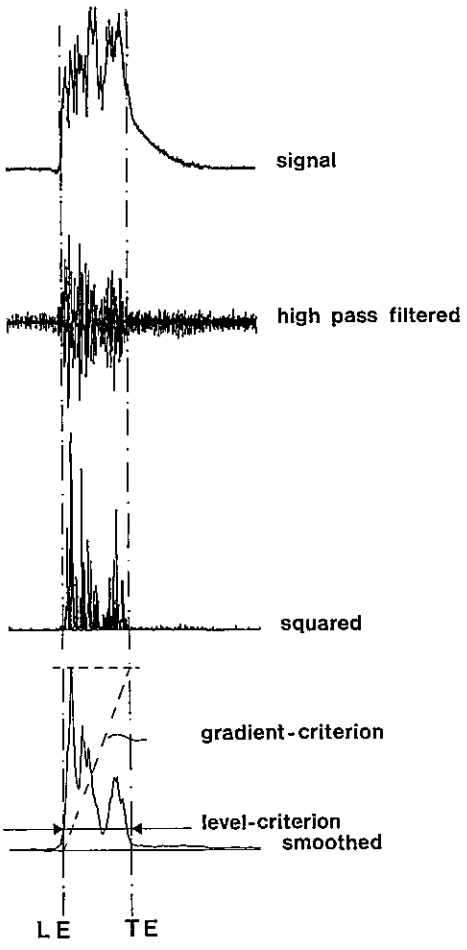

Fig. 2. Detection scheme for the determination of spot leading and trailing edge as applied to the *U*-velocity-signal.

structures becomes a factor of two smaller for $N = 90$. We anticipate that the small-scale structures are randomly distributed throughout the ensemble and that in the limit $N \to \infty$ we would end-up with a fairly smooth average. Another reason for losing small-scale structures in the ensemble average is the variation of the spot length throughout the ensemble. This variation is of the order of 5 ms, which means that scales smaller than 5 ms cannot survive in the ensemble average.

Since there is no significant information in the average on scales smaller than 5 ms we can take 60 realisations and smooth the average with a low-pass filter with a cut-off frequency of 200 Hz.

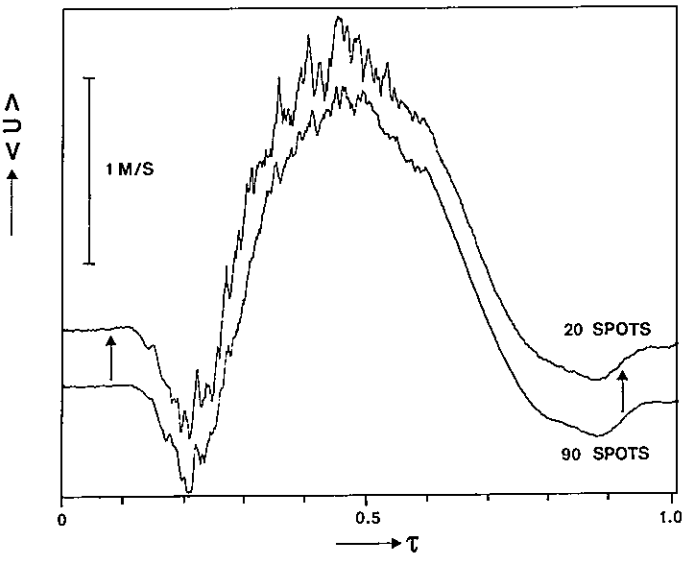

Fig. 3. The influence of the number of spot realisations on the ensemble average (origin translated as indicated by arrows). $U_0 = 8.35\,\text{m/s}$, $x = 0.70\,\text{m}$, $y = 2.0\,\text{mm}$ and $z = 0\,\text{mm}$.

Working with ensemble averages, we have to define what we mean by ensemble-averaged stress $\langle uv \rangle$. The instantaneous velocity signal X ($= U$ or V) is split into three parts:

$$X = X_1 + \langle X \rangle + x,$$

where X_1 the laminar flow-velocity,
$\langle X \rangle$ the ensemble averaged excess velocity,
x the fluctuating part.

The ensemble averaged stress is defined as the covariance of the fluctuating parts of U and V, i.e. $\langle uv \rangle$. Due to different y-positions of the two measuring centres of the X-wire probe an apparent V-velocity is introduced which is proportional to $\partial_y U$. Corrections for this are made in the ensemble average. For the lowest measuring station the gradient is unknown, so $\langle V \rangle$ and $\langle uv \rangle$ at this level are removed from the data-set.

4. Results

U- and V-measurements are made at $x = 0.85\,\text{m}$, at $z = 0, \pm 15, \pm 30, \pm 45$ and $\pm 60\,\text{mm}$ at several y-positions between 0.75 and 16 mm. The spot

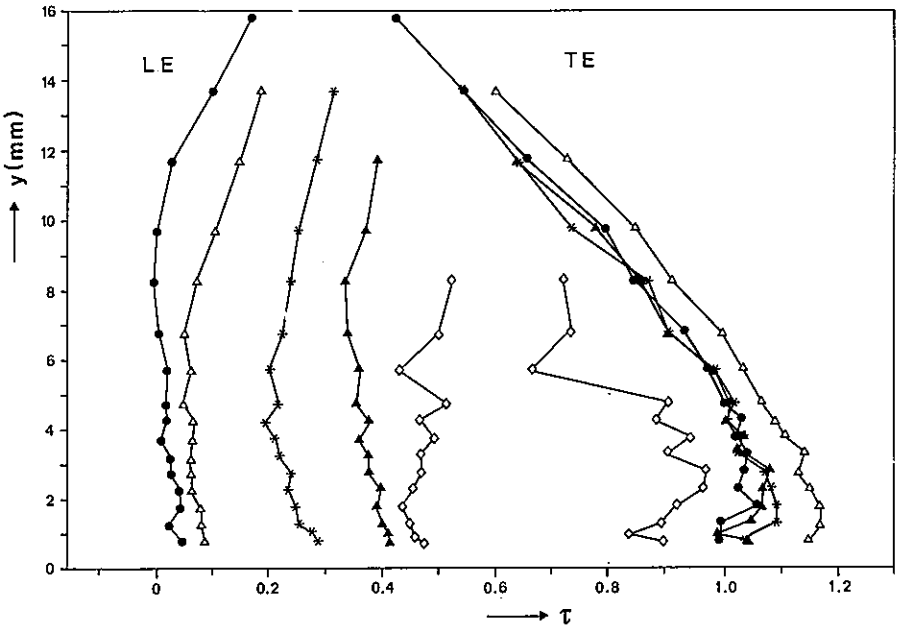

Fig. 4. The turbulent spot-edges in the y-τ plane. $U_0 = 8.35$ m/s, $x = 0.85$ m. ●: $z = 0$ mm, △: $z = 15$ mm, ∗: $z = 30$ mm, ▲: $z = 45$ mm, ◇: $z = 60$ mm.

turned out to be symmetrical, so only the results for $z > 0$ mm are presented. In the figures discussed in this section and in Section 5, the time-origin is chosen to be the first spot arrival, which is at $z = 0$ mm, $y = 8.25$ mm. The average time between the trigger signal and the spot arrival time (t_{arr}) is 128 ms. The time coordinate is made dimensionless according to $\tau = (t - t_{arr}) \cdot U_0/(x - x_w)$, where x_w denotes the position of the tripping wire. All figures represent ensemble-averaged properties of 60 realisations. The position of the LE and TE in the y-τ plane are shown in Fig. 4, while those in the z-τ plane are shown in Fig. 5. The edges of the spot resemble those measured by [12], although the overhang for $z = 0$ mm is less pronounced here. For $z = 60$ mm at the higher levels it appears that the LE- and TE-detection criteria break down. This is mainly due to the large variation in detected spot-lengths at these positions. U_{LE} and U_{TE} are calculated from the differences in arrival times of the spot edges at $x = 0.70$ m and $x = 0.85$ m. In the plane of symmetry $U_{LE} = 0.77 \cdot U_0$ near the wall, while $U_{TE} = 0.50 \cdot U_0$ [10] found a somewhat higher U_{LE} of $0.90 \cdot U_0$, and the same value for U_{TE}.

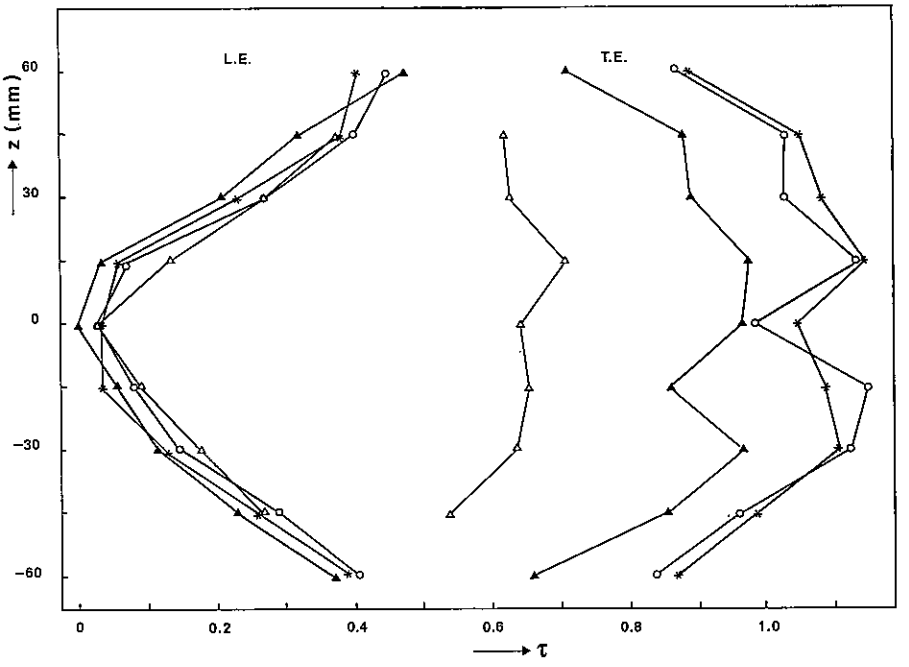

Fig. 5. The turbulent spot-edge in the z-τ plane. $U_0 = 8.35$ m/s, $x = 0.85$ m. ○: $y = 0.86$ mm, ∗: 1.75 mm, ▲: $y = 6.75$ mm, △: $y = 11.75$ mm.

Figures 6, 7 and 8 show the ensemble-averaged $\langle U \rangle$, $\langle V \rangle$ and $\langle uv \rangle$-distributions, respectively. Dots indicate the position of LE and TE at each recorded position. In this section we compare our measurements at $z = 0$ mm with the ones performed by [2]. Their test conditions were: $U = 11\,m/s$, spot generation by a spark at $x = 29$ cm, measurement position at $x = 113$ cm.

Figure 6a–e gives $\langle U \rangle$-velocities in the y-τ plane for the positive z-positions. Near the wall a rapid increase in $\langle U \rangle$ is found at the LE, which continues more slowly towards the TE. For higher y-positions, $\langle U \rangle$ shows a sharp decrease at the LE followed by a slow return to the laminar value near the TE. At $z = 0$ mm, for $2 < y < 4$ mm, this negative dip is preceded by a small positive value. These features may also be observed from Fig. 9, where isotachs of $\langle U \rangle$ are drawn for $z = 0$ mm. The absolute minimum $\langle U \rangle = -2.0$ m/s is at $y = 3.75$ mm, $z = 0$ mm, in agreement with results of [2]. The absolute maximum $\langle U \rangle = 3.0$ m/s is reached at $y = 0.76$ mm, $z = 0$ mm. Time gradients have values of $\partial \langle U \rangle / \partial t = 150$ m/s^2 at the LE with an absolute maximum of 500 m/s^2 at $y = 0.76$ mm, $z = 0$ mm. When leaving the plane of symmetry, the area of $\langle U \rangle$-velocity surplus expands slightly upwards from $y = 1.75$ mm, $z = 0$ mm to

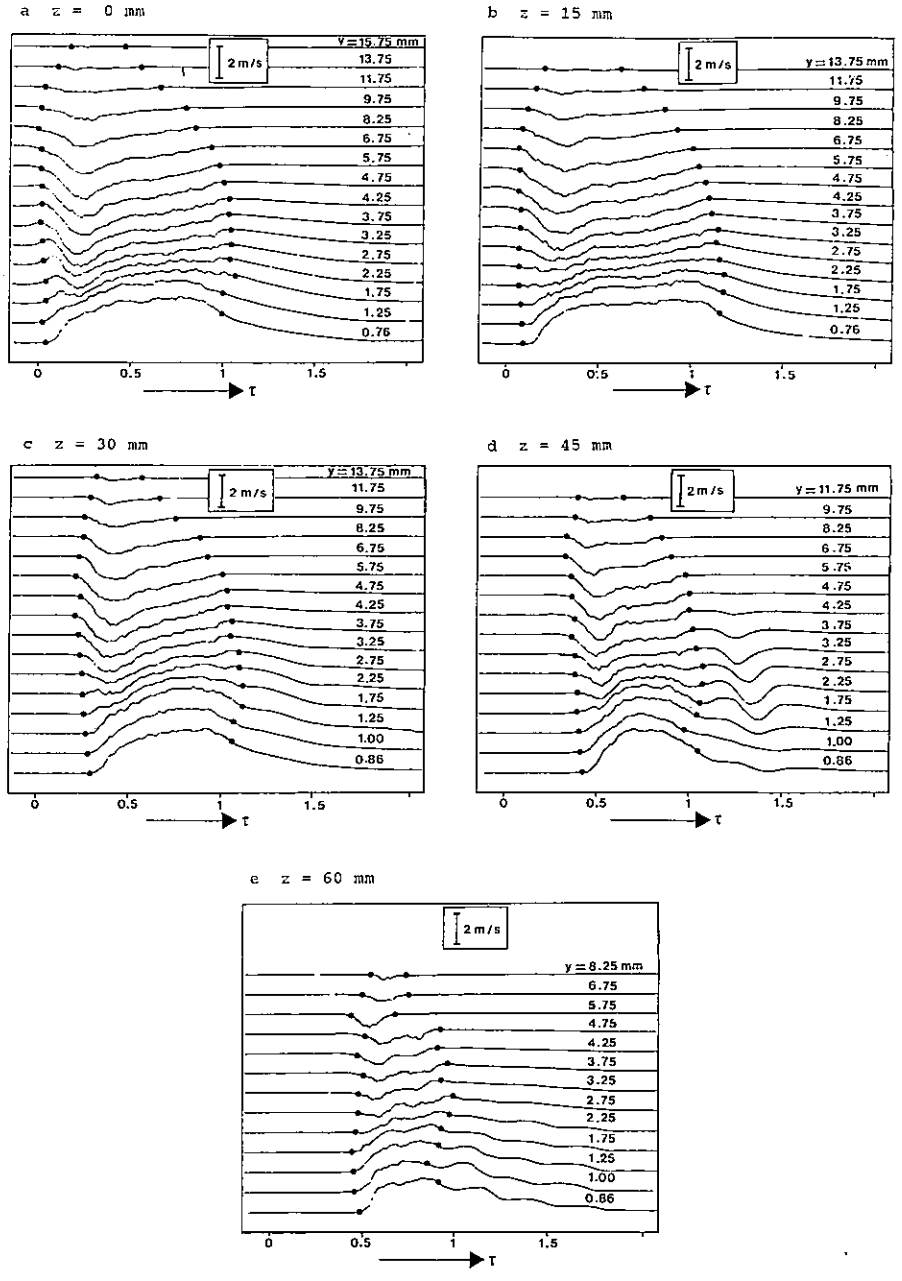

Fig. 6. The ensemble-averaged U-excess-velocity distribution at the position $x = 0.85\,\text{m}$, $U_0 = 8.35\,\text{m/s}$ for different heights y. The vertical bar indicates the $\langle U \rangle$-scale; the undisturbed lines in front of the spot indicate the $\langle U \rangle = 0$ level for each height. a: $z = 0\,\text{mm}$, b: $z = 15\,\text{mm}$, c: $z = 30\,\text{mm}$, d: $z = 45\,\text{mm}$, e: $z = 60\,\text{mm}$.

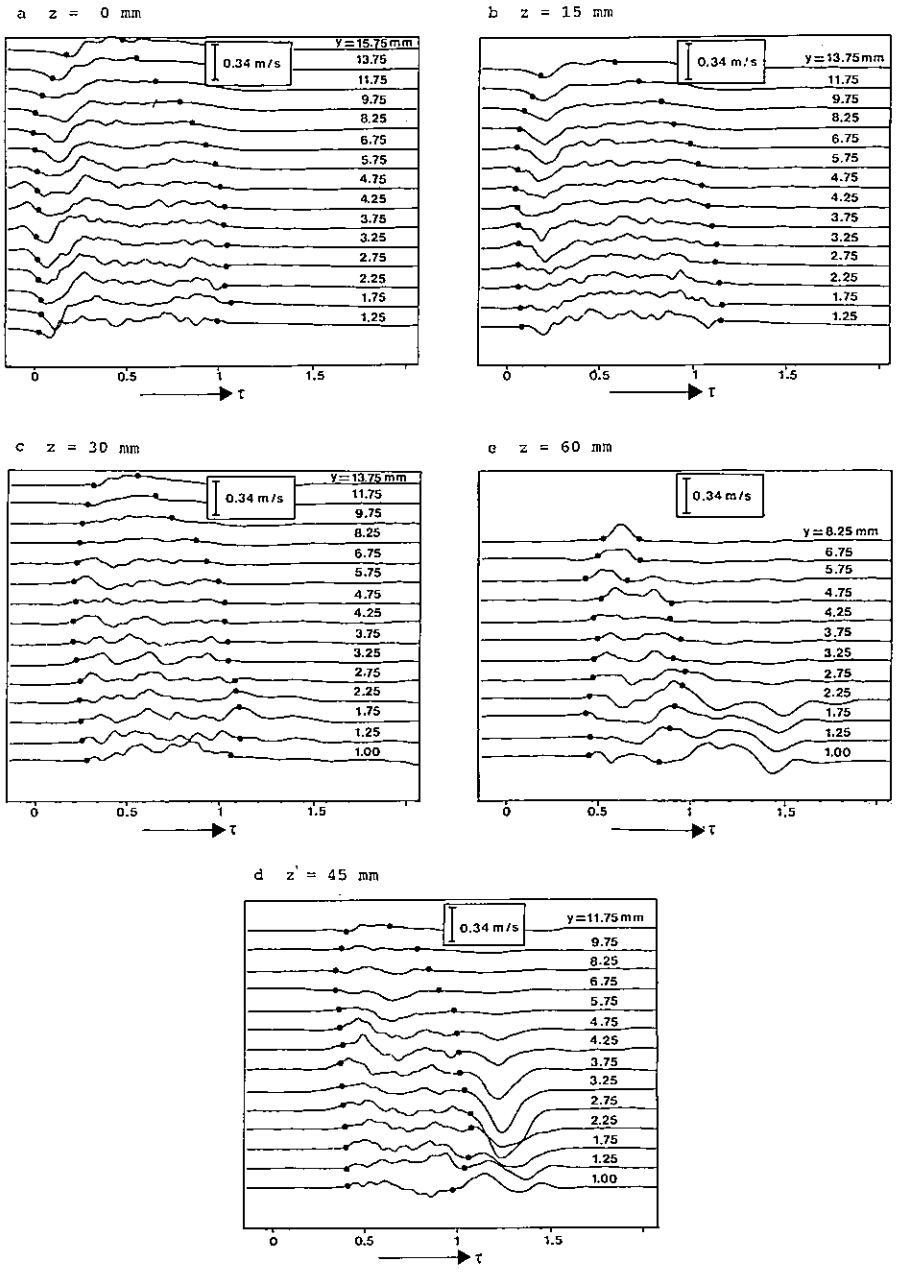

Fig. 7. The ensemble averaged $\langle V \rangle$-velocity distribution at the position $x = 0.85\,\mathrm{m}$, $U_0 = 8.35\,\mathrm{m/s}$, for different heights y. The vertical bar indicates the $\langle V \rangle$-scale; the undisturbed lines in front of the spot indicate the $\langle V \rangle = 0$ level for each height. a: $z = 0\,\mathrm{mm}$, b: $z = 15\,\mathrm{mm}$, c: $z = 30\,\mathrm{mm}$, d: $z = 45\,\mathrm{mm}$, e: $z = 60\,\mathrm{mm}$.

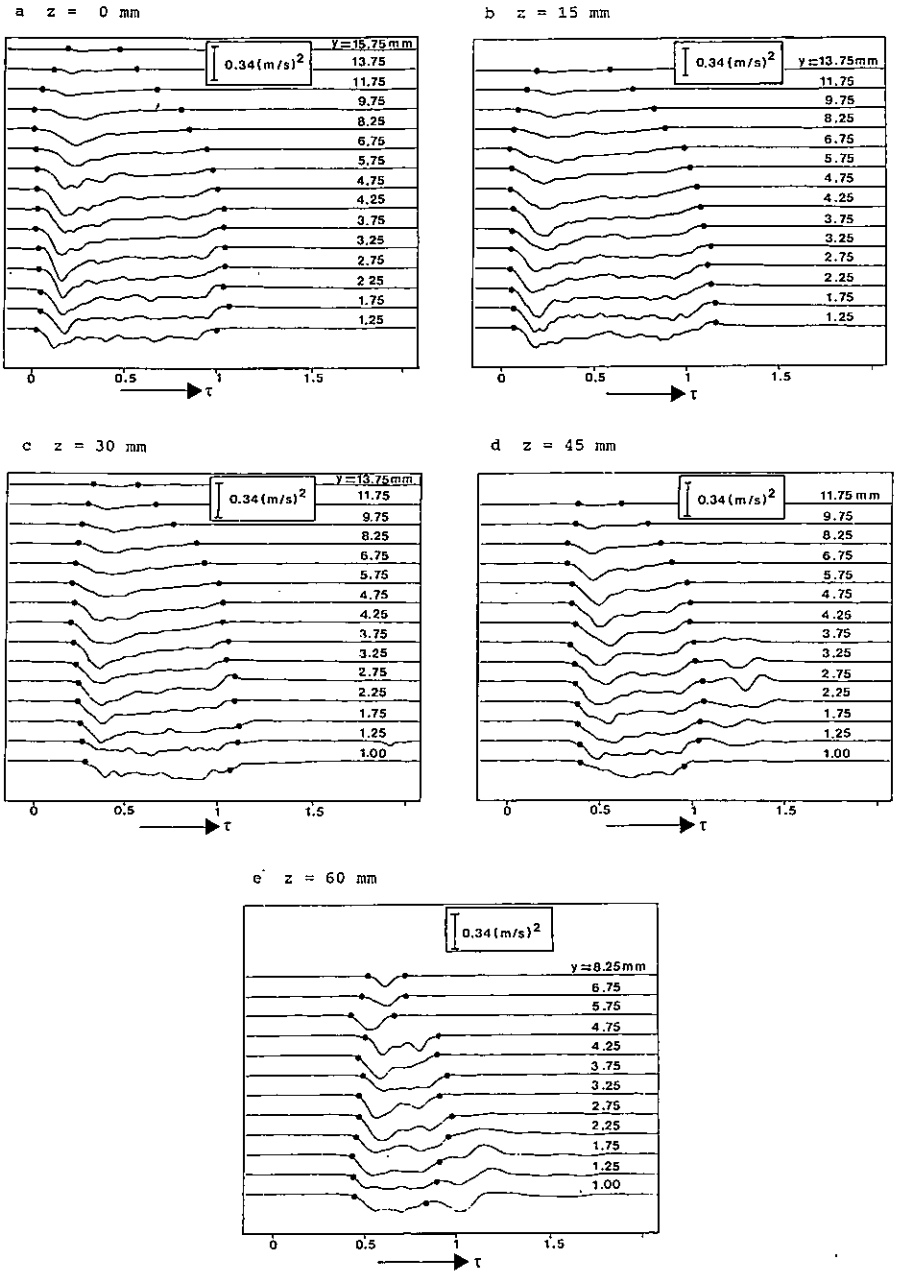

Fig. 8. The ensemble averaged $\langle uv \rangle$-distribution at the position $x = 0.85\,\text{m}$, $U_0 = 8.35\,\text{m/s}$, for different heights y. The vertical bar indicates the $\langle uv \rangle$-scale; the undisturbed lines in front of the spot indicate the $\langle uv \rangle = 0$ level for each height. a: $z = 0\,\text{mm}$, b: $z = 15\,\text{mm}$, c: $z = 30\,\text{mm}$, d: $z = 45\,\text{mm}$, e: $z = 60\,\text{mm}$.

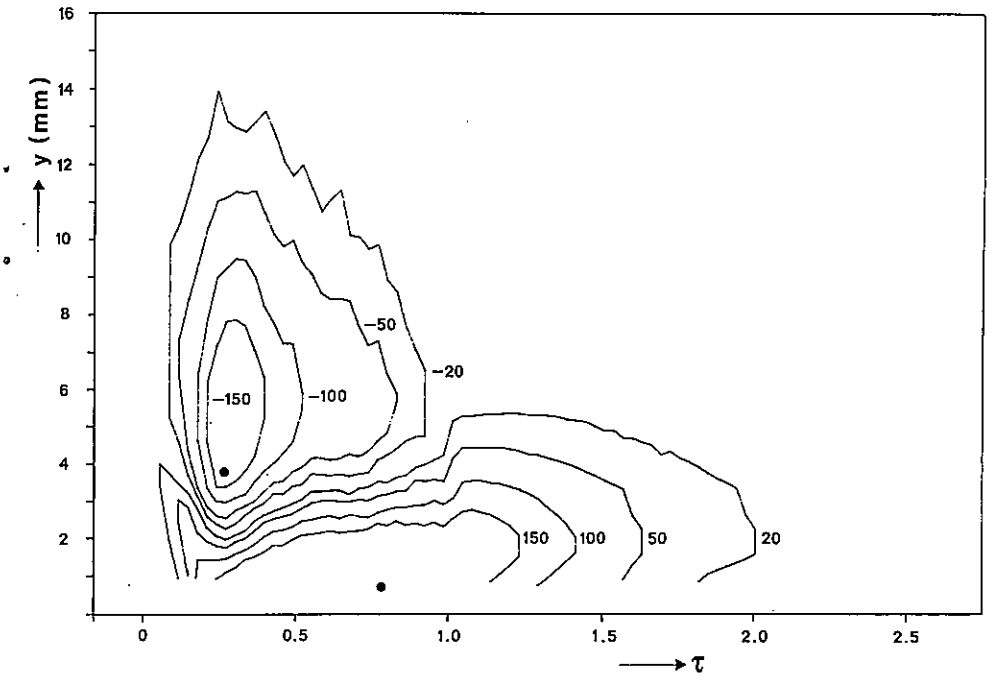

Fig. 9. $\langle U \rangle$-isotachs (in cm/s) at $x = 85$ m, $z = 0$ m, $U_0 = 8.35$ m/s. The circles indicate the minimum (-200 cm/s) and maximum (300 cm/s) values.

$y = 2.75$ mm at $z = 60$ mm. Near the TE, up to $y = 5$ mm, $\langle U \rangle$ is larger than the laminar value. In Fig. 6 waves can be observed at $z = 30$, 45 and 60 mm. These waves are in phase throughout the ensemble. Individual records show the same $\langle U \rangle$ amplitudes of about 0.5 m/s as the ensemble average. The wave period is approximately 20 ms. At $z = 45$ and 60 mm a phase shift seems to occur going downward from $y = 1.25$ mm to 0.86 mm. These waves seem to be a forced oscillation of the boundary layer. Chambers and Thomas [4] visualized these trailing Tollmien-Schlichting waves, Wygnanski et al. [11] argued that at $z = 0$ mm these waves are not present because the trailing velocity profile is more convex and thus more stable.

Figure 7a–e shows $\langle V \rangle$-velocities. Near $z = 0$ mm a negative "dip", often preceded by a small positive $\langle V \rangle$-value, occurs at the LE, followed by a positive $\langle V \rangle$. Though diminishing, this positive $\langle V \rangle$ remains towards TE. The negative dip has its absolute minimum $\langle V \rangle = -0.21$ m/s at $z = 0$ mm, $y = 1.75$ mm. This value is similar to the one measured by [2]. Outward towards larger z-values the negative dip disappears. $\langle V \rangle$ shows positive values throughout the spot with small local maxima near the LE and/or TE.

Reynolds-stresses $\langle uv \rangle$ are shown in Fig. 8a–e. At all positions $\langle uv \rangle$ is negative. At almost all y-stations a sharp negative "dip" occurs at the LE, followed by a period of nearly constant $\langle uv \rangle$. The $\langle uv \rangle$-field shows the same characteristics as found by [2]. The period of nearly constant $\langle uv \rangle$ is only found close to the wall by [2]. The absolute minimum of $\langle uv \rangle = -0.32\,(\mathrm{m/s})^2$ is found at $z = 0\,\mathrm{mm}$, $y = 3.25\,\mathrm{mm}$. As all gradients tend to get smaller outside the plane of symmetry, the overall picture remains the same, except at $z = 60\,\mathrm{mm}$, where for $y > 2\,\mathrm{mm}$ the period of constant $\langle uv \rangle$ is hardly apparent. At these positions a second minimum in $\langle uv \rangle$ is found near the TE.

In general, our measurements at $z = 0\,\mathrm{mm}$ lead to the same results as found by [2]. However, some differences occur especially in $\langle V \rangle$- and $\langle uv \rangle$-measurements.

5. Discussion and interpretation of the results

The turbulent spot is embedded in a highly sheared velocity field. We observe a fairly organized turbulent region which moves downstream at a velocity less than U_0. This observation leads to the assumption that strong mechanisms are working which prevent the turbulent structure from being blown about.

Although it is known that in individual spots vigorous mechanisms such as bursting play an important role, it is obvious that for the ensemble averaged structure only the influences described by the Reynold-stresses are important. The processes in individual spots remain to be related with the ensemble-averaged Reynolds-stress.

Here we are limiting ourselves to the ensemble-averaged spot and try to explain the relation between the $\langle U \rangle$-, $\langle V \rangle$-field and the $\langle uv \rangle$-field (which is the dominant stress in turbulent boundary layer processes) in a qualitative way.

In Fig. 10a the profiles of $\langle U \rangle$ are displayed for the first half of the spot. We see that the Blasius-profile is quickly distorted to a typical turbulent boundary layer profile. The near-logarithmic profiles in the centre of the spot correspond to a stress value of $-0.35\,(\mathrm{m/s})^2$, which is about the stress measured at the LE of the spot. In the transition phase from Blasius to logarithmic profiles a sharp vertical gradient is observed at $y \approx 4\,\mathrm{mm}$.

Figure 10b shows the stress profiles throughout the spot. An overhang is observed at the LE of the spot. Further behind the LE the profiles show a more or less constant flux layer up to $y \approx 4\,\mathrm{mm}$. The overhang in the stress gives rise to a strong acceleration of air near the wall, as can be seen in Fig. 6a. At higher levels air overtakes the TE, which moves at a speed of $0.5 \cdot U_0$. This air is decelerated by the gradient of the shear stress. Due to

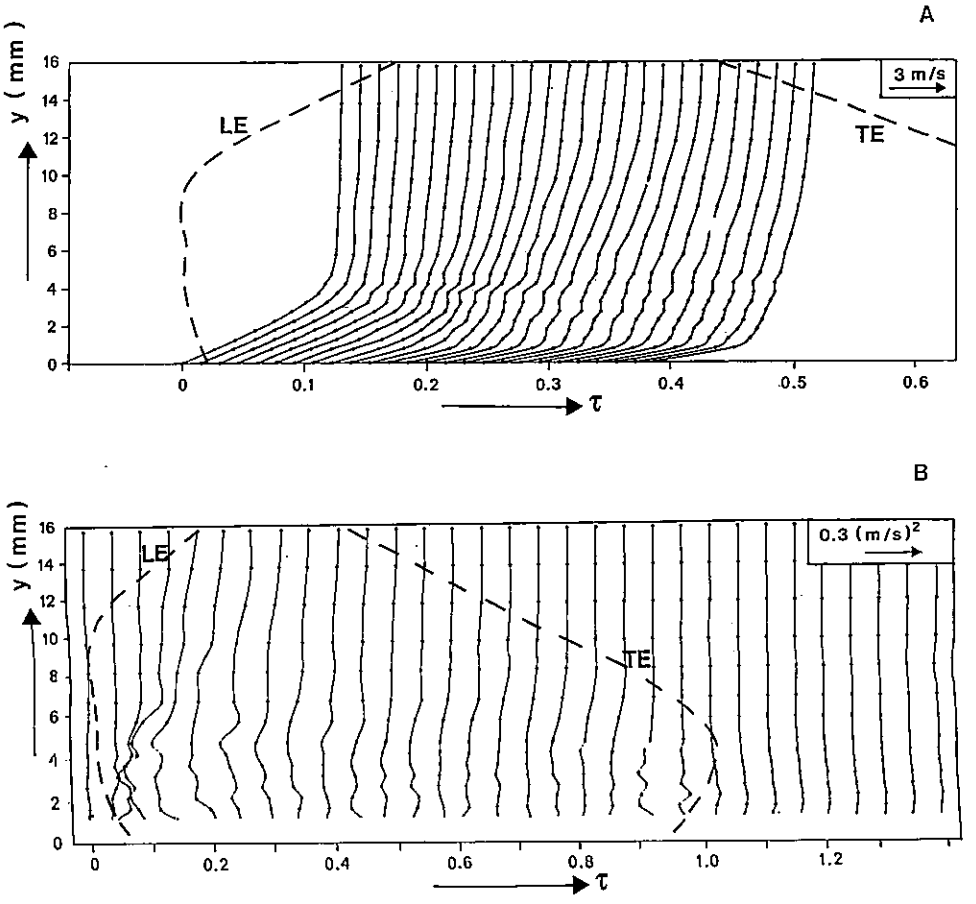

Fig. 10. $\langle U \rangle$-velocity profiles (10.a) and $\langle uv \rangle$-stress profiles (10.b) at $x = 0.85$ m, $z = 0$ mm, $U_0 = 8.35$ m/s. Dashed lines indicate LE or TE, reproduced from Fig. 4.

stagnation the air attains an upward motion (Fig. 7a). Upstream of the LE the velocity is undisturbed and larger than inside the spot. Owing to continuity there must be a downward motion near the LE, as can be seen in Fig. 7a. It seems that the downward motion is so strong that high $\langle U \rangle$-velocity is transported downward resulting in the maxima in $\langle U \rangle$ at the LE for $y \approx 3$–4 mm. Since the downward motion corresponds to $d\langle V \rangle/dy < 0$, the already present shear in $\langle U \rangle$ is intensified. This corresponds to the strong gradient in Fig. 10a.

It can be deduced that the turbulent kinetic energy production takes place at a rate equal to the product of the shear stress and the vertical shear of the horizontal velocity. If we assume that regions with high production rates

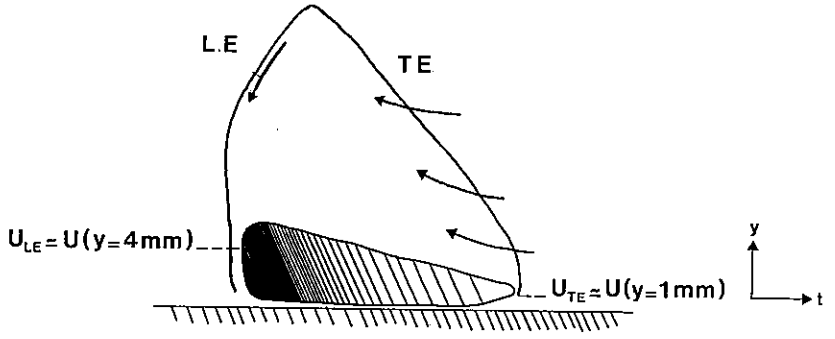

Fig. 11. Structure of the turbulent spot. Arrows indicate in- and outflow through TE and LE respectively. The shaded area represents the high turbulence intensity core of the spot.

correspond to regions with high turbulent intensities, we can conclude from the figures 10a and 10b that this region in the spot reaches from about $y \approx 4$ mm at the LE to $y \approx 1$ mm at the TE. Now, the advection velocities at these levels correspond well with U_{LE} and U_{TE} respectively. So we end up with a spot structure as shown in Fig. 11, where it is assumed that the high intensity region is advected by the local velocity and this region is sustained by the kinetic energy production at the levels where stress times shear is high. The fact that $U_{LE} < U_0$ also indicates that at the LE for large y-values the downward $\langle V \rangle$-velocity is so high that no outflow through the LE occurs.

Outside the plane of symmetry all features become less pronounced. The sharp dips in the $\langle uv \rangle$- and $\langle V \rangle$-signal and the high shear near the LE of the spot gradually disappear. This suggests that other mechanisms are at work here to achieve transition of the laminar flow. It is suggested by [5] that pressure-induced destabilisation of the conditionally stable boundary layer is the important mechanism here.

Acknowledgement

We thank Prof. F.T.M. Nieuwstadt for his stimulating advice.

References

1. Amini, J. and Lespinard, G: Experimental study of an "incipient spot" in a transitional boundary layer. Chambers, A.J., Sokolov, M. and Van Atta C.W.: *Phys. Fluids* 25 (1982) 1743.
2. Antonia, R.A., Chambers, A.J., Sokolov, M. and van Atta, C.W.: Simultaneous temperature and velocity measurements in the plane of symmetry of a transitional turbulent spot. *J. Fluid Mech.* 108 (1981) 317.

3. Cantwell, B., Coles, D. and Dimotakis, P.: Structure and entrainment in the plane of symmetry of a turbulent spot. *J. Fluid Mech.* 87 (1978) 641.
4. Chambers, F.W. and Thomas, A.S.W.: Turbulent spots, wave packets and growth. *Phys. Fluids* 26 (1983) 1160.
5. Gad-el-Hak, M., Blackwelder, R.F. and Riley, J.J.: On the growth of turbulent regions in laminar boundary layers. *J. Fluid Mech.* 110 (1981) 73.
6. Henningson, D., Spalart, P. and Kim, J.: Numerical simulations of turbulent spots in plane Poiseuille and boundary-layer flow. *Phys. Fluids* 30 (1987) 2914.
7. Itsweire, E.C., van Atta, C.W.: An experimental investigation of coherent substructures associated with turbulent spots in a laminar boundary layer. *J. Fluid Mech.* 148 (1984) 319.
8. Mantuer, T.S. and van Atta, C.W. An experimental study of the wall-pressure field associated with a turbulent spot in a laminar boundary layer. *J. Fluid Mech.* 118 (1982) 59.
9. Strohl, A. and Comte-Bellot, G.: Aerodynamic effects due to configuration of wire characteristics. *J. Applied Mech.* 40 (1973) 661.
10. Wygnanski, I.: The effect of Reynolds number and pressure gradient on the transitional spot in a laminar boundary layer. Jimenez, J. (ed.), In: *The Role of Coherent Structures in Modelling Turbulence and Mixing*. Lecture notes in Physics (1981) no. 136, p. 304.
11. Wygnanski, I., Haritonidis, J.H. and Kaplan, R.E.: On a Tollmien-Schlichting wave packet produced by a turbulent spot. *J. Fluid Mech.* 92 (1979) 505.
12. Wygnanski, I., Sokolov, M. and Friedman, D.: On a turbulent 'spot' in a laminar boundary layer. *J. Fluid Mech.* 78 (1976) 785.
13. Wygnanski, I., Zilberman, M. and Haritonidis, J.H.: On the spreading of a turbulent spot in the absence of a pressure gradient. *J. Fluid Mech.* 123 (1982) 6.
14. Zilberman, M.: On the interaction of transitional spots and generation of a synthetic boundary layer, PhD-thesis, Tel Aviv (1982).